55TH EASTERN SNOW CONFERENCE
Jackson, New Hampshire 1998

The Association Between Spatially Autocorrelated Patterns of SSM/I Derived Prairie Snow Cover and Atmospheric Circulations

C. DERKSEN[1], M. WULDER[2], E. LEDREW[1], AND B. GOODISON[3]

ABSTRACT

Passive-microwave derived observations of snow cover show potential to provide synoptically sensitive, and hydrologically and climatologically significant information because of all-weather imaging capabilities, rapid scene revisit time, and the ability to derived quantitative estimates of snow water equivalent (SWE). In this study, we seek to identify the dominant patterns of clustering in SWE imagery using the Getis statistic, a local indicator of spatial association. The SWE data were derived from five day averaged Special Sensor Microwave/Imager (SSM/I) brightness temperatures using the Canadian Atmospheric Environment Service dual channel algorithm. The analyzed data span one winter season (December, January, and February 1988/89) and are limited to a ground validated Prairie scene. National Center for Environmental Prediction (NCEP) gridded atmospheric data (500 mb geopotential height; 700 mb temperature) were incorporated into the study to investigate whether the spatial orientation of the Getis statistic clusters provides information on interaction between snow cover and the atmosphere. Results show that the direction of atmospheric airflow as expressed by the 500 mb geopotential height field corresponds strongly to the orientation of surface snow cover clusters with no time lag. The 700 mb temperature field is also a controlling influence on the snow cover clusters both by modifying cluster orientation, and reinforcing cluster magnitude.

Key words: passive-microwave, snow water equivalent, spatial autocorrelation, atmospheric interaction.

INTRODUCTION

Terrestrial snow cover undergoes the largest spatial and temporal fluctuations of any surface cover on the earth (Cohen, 1994). With unique physical properties such as an extremely high surface albedo, variability in snow cover extent has climatological implications at local, regional, and global scales. As the frozen storage term in the water balance, snow cover plays an important role in the hydrologic cycle, while the presence or absence of snow also influences evaporation and runoff, and serves a biological role as species habitat (Karl et al., 1993). General circulation models struggle to accurately portray the snow-albedo feedback mechanism which can control the regional absorption of shortwave radiation (Cess et al., 1991), while there is also disagreement on the implications of a changing climate on crysopheric variables (Washington and Meehl, 1986; Flato, 1997). Quantitative information on snow distribution and depth is therefore required for a diverse range of applications.

In this study, an algorithm developed by the Canadian Atmospheric Environment Service (AES) is applied to Special Sensor Microwave/Imager (SSM/I) brightness temperatures to create a time series of snow water equivalent (SWE) images. An analysis subscene composed of the Canadian Prairies and American Great Plains is used as the SWE algorithm is validated for Prairie surfaces only. While the restrictive spatial application of the SSM/I data is a clear limitation, the all-weather imaging capability of the passive microwave sensor provides improvements over snow cover products derived from optical sensors. Rapid revisit time of the SSM/I sensor also allows for fine temporal resolution -- in this case five day averaged data (pentads). The Prairie region is an ideal area for which to begin exploring snow cover/atmospheric interactions, as this is a very active region with respect to the variability of snow cover frequency and persistence (Leathers and Robinson, 1993). At present, SSM/I data in the EASE (Equal Area SSM/I Earth) grid format have been officially released for the period August 1987 to June 1990 only, which hampers time series analysis, but is adequate for the evaluation of analysis techniques.

We seek to exploit the information contained in SSM/I derived SWE images of the Canadian Prairies and American Great Plains through the use of the Getis statistic (G_i^*), a local indicator of spatial association. A single winter of data (December, January, February, 1988/89) are examined at temporal resolution of five

[1] Waterloo Laboratory for Earth Observations, Department of Geography, University of Waterloo, Waterloo, Ontario N2L 3G1, Canada
[2] Pacific Forestry Centre, 506 West Burnside Road, Victoria, British Columbia V8Z 1M5, Canada
[3] Climate Research Branch, Atmospheric Environment Service 4905 Dufferin Street, Downsview, Ontario M3H 5T4, Canada

days. This sequence of data allows for evaluation of the Getis statistic as an effective means of identifying spatial patterns within SWE images. The specific objectives are as follows: (1) to identify the dominant clustering patterns within the SWE imagery through the winter season using the Getis statistic; (2) to isolate the orientation of the snow cover clusters (for example north to south, east to west) through the winter season; (3) to link the snow cover cluster orientation to coincident atmospheric circulation patterns.

DATA

SSM/I Derived Snow Water Equivalent

Regional scale climatological and hydrological snow cover studies require spatially and temporally sensitive data sets to monitor the evolution of snow cover over time. While the longest existing data sets are based on station measurements, these point data require spatial interpolation and can be hindered by inaccurate and biased measures (see Brown and Goodison, 1996). Remotely sensed data has therefore been utilized because of its ability to provide repetitive data for large regions. Optical imagery from NOAA satellites has provided a North American snow cover product since 1966. The NOAA snow charts, however, are based on visual interpretation, and are influenced by problems ranging from cloud masking issues to surface cover (such as forests) blocking the identification of snow deposition (Wiesnet et al., 1987). Finally, the NOAA product provides binary snow/no snow grid output, with no information with respect to snow depth.

Passive microwave imagery has therefore been explored as a potential snow cover data source. Passive microwave imagers have been in orbit since 1972 when the Electronic Scanning Multichannel Radiometer (ESMR) was launched. Snow cover retrieval algorithms have subsequently been created for Scanning Multichannel Microwave Radiometer (SMMR -- launched in 1978) brightness temperatures (for example Chang et al., 1987), and SSM/I data (for example Goodison, 1989; Grody and Basist, 1996).

The ability to estimate SWE in the microwave portion of the electromagnetic spectrum is a function of changes in microwave scatter caused by the presence of snow crystals. For a snow covered surface, the brightness temperature (T_b) decreases with increasing snow depth because the greater number of snow crystals provides increased scattering of the microwave signal.

This simple relationship is complicated by factors associated with snow grain size. An increase in grain size increases the scattering cross-section, thereby lowering the microwave brightness temperature. This artificially implies an increase in snow amount. Armstrong et al. (1993), found that a change in snow grain diameter of 0.4 mm results in a change in brightness temperature of 50 ° Kelvin. This sensitivity to grain size occurs through a range of grain diameters, from 0.1 mm to 1.0 mm, the maximum field measured diameter (Armstrong et al., 1993). The presence of depth hoar, or large faceted grains, has been found to be a great source of error in microwave retrieval of snow cover parameters (Chang et al., 1987; Hall et al., 1991). These large crystals develop when the snowpack temperature gradient exceeds 10°C m^{-1} (Colbeck, 1987). The disproportionate size of depth hoar to other snow grains, skews the relationship between brightness temperature and snow depth. Since the decrease in T_b due to snow depth and the decrease in T_b due to depth hoar are not additive (Hall et al., 1991), the influence of depth hoar on microwave scatter is not easily accounted for.

Other influences on snowpack scattering include the properties of the underlying soil, vegetation cover, and atmospheric conditions. Ulaby and Stiles (1980) found that the backscattering coefficient and emissivity of snow are dependent not only on the snowpack water equivalent, but the underlying soil type and wetness, while Kurvonen and Hallikainen (1997) found that land cover type strongly influences the emissivity of snow covered ground. Airborne studies have indicated that higher microwave wavelengths (greater than 94 GHz) are ideal for monitoring snow cover (Kurvonen and Hallikainen, 1997). However these wavelengths are not atmospherically transparent and are therefore not utilized by spaceborne satellite sensors.

Finally, a wet snowpack limits quantitative determination of SWE, even hampering discrimination between melting snow areas and snow free land (Walker, 1993). As snow wetness increases, the brightness temperature increases, approaching black-body behaviour at vertical polarizations. Attempts to use a polarization gradient to monitor SWE can therefore produce erroneous under-estimateswhen the snowpack is wet.

AES has developed and evaluated single and dual channel algorithms for determining SWE for prairie regions using passive microwave data. Goodison and Walker (1994) outline the use of the algorithms and their strengths and weaknesses for these areas. The AES dual frequency algorithm used in this study utilizes the vertically polarized 19 and 37 GHz channel brightness temperatures (25 km spatial resolution), and was developed through an intensive satellite/airborne/ground based experiment in the Canadian Prairies (Goodison et al., 1986). SWE is calculated based on the commonly

used form of the relationship between SWE and brightness temperature:

$$SWE = a + b\Delta T_B$$

where, for SSM/I data, a = -20.7, b = -2.74, and ΔT_B is the difference between 37GHz and 19GHZ vertically polarized brightness temperatures (Goodison and Walker, 1994).

Northern Hemisphere SWE imagery were derived from SSM/I brightness temperatures in the EASE (Equal Area SSM/I Earth) Grid projection provided by the National Snow and Ice Data Center in Boulder, Colorado. From the EASE-Grid projection, a study area (60 by 60 = 3600 pixels) composed of the Canadian Prairies and American Great Plains was selected for analysis (Figure 1). Before algorithm processing, the brightness temperatures were combined into five day averages (pentads) which is a compromise between the need to construct a time series of acceptable synoptic sensitivity, and ensuring complete scene coverage.

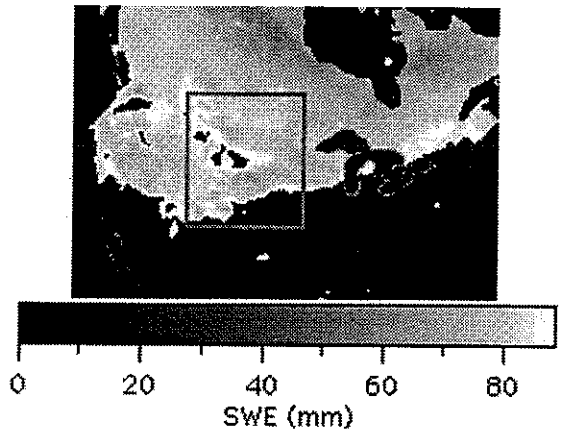

Figure 1.Subset of Northern Hemisphere SWE image, with Prairie study area outlined. Image is a composite of January 1 to January 5, 1989.

Due to the factors discussed previously, algorithm performance is strongest when snowpack conditions are thick and dry, achieving 10 to 20 mm agreement with surface sampling. Problems occur when fresh snow is deposited on a warm surface, and when attempting to discriminate between melting snow areas and snow free land (Walker and Goodison, 1993). For these reasons, the winter months of December, January, and February were selected for analysis. Data from ascending orbits only were used as these overpass times are in the morning, thereby mitigating the influence of melt.

Atmospheric Data

Atmospheric data from the National Center for Environmental Prediction (NCEP, formerly National Meteorological Center - NMC) were acquired for analysis. These data are projected onto a 1977 point octagonal grid, with equal spaced points when viewed polar stereographically. A 324 point data coverage (18 by 18) was removed from the original grids for analysis. The atmospheric data study area is larger than the SSM/I scene in order to examine connections to atmospheric conditions spatially removed from the region of ground validated SWE data. For the scope of this work, only two atmospheric variables will be utilized: 500 mb geopotential height (500Z) and 700 mb temperature (700T). 500Z was selected because it approximates both the jet stream with no surface influence, and the mean level of non-divergence. Likewise, 700T is not influenced by the surface and provides an indicator of thermal advection.

METHODS

Spatial autocorrelation can be defined as the strength of the relationship between values of the same variable at nearby locations. When similar values are clustered in close proximity, positive spatial autocorrelation is present, while negative spatial autocorrelation occurs when neighbouring values are dissimilar (Goodchild, 1986). Measures of spatial autocorrelation are either global or local in nature. Global measures provide a single value which summarizes the level of spatial autocorrelation within the variable distribution, while local indicators of spatial association are able to deconstruct a single global measure by providing a value of spatial autocorrelation for each location within the variable distribution (Anselin, 1995). The Getis statistic is one such local indicator (Getis and Ord, 1992; Ord and Getis, 1995). While the Getis statistic was originally created for point data, recent research shows that it can be successfully applied to remotely sensed imagery (Wulder and Boots, 1998).

The Getis statistic expresses the sum of the variate values within a specified distance from a single point as a proportion of the sum of the variate values for the entire study area. There are two versions of the Getis statistic: G_i and G_i^*. G_i does not include the point of interest from the local sum, while G_i^* does. G_i^* is more appropriate for remote sensing applications because it allows computation of the statistic using a defined window size around a centre pixel. The equation for G_i^*, with the output values being similar to standardized Z scores, is as follows:

$$\frac{G_i^*(d) = \Sigma_j w_{ij}(d)x_j - W_i^* \overline{x}}{s[W_i^*(n-W_i^*)/(n-1)]^{1/2}}$$

where $\Sigma_j w_{ij}(d)x_j$ is the sum of the variates within distance d of observation i, including i, W_i^* is the count of the pixels within distance d of pixel i, including i, $\overline{x}$ is the global mean, s is the global standard deviation, n is the total number of observations.

G_i^* was calculated for each pixel in the Prairie SWE imagery at four distances: d =1, 2, 3, and 4. This corresponds to window sizes of 3x3, 5x5, 7x7, and 9x9 pixels respectively. The largest standardized G_i^* value for the four distances represents the maximization of local association, therefore the maximum G_i^* value for each pixel was retained and written to an image file for further investigation. Large positive G_i^* values indicate a cluster of high pixel values, while large negative values denote clusters of low pixel values. This interpretation is different from other measures of spatial autocorrelation where clustering of both high and low values result in positive values of spatial autocorrelation. A weakness of the Getis statistic is that clustering of average pixel values cannot be determined: if a G_i^* value of near zero is calculated it can be attributed to either a cluster of average values, or a lack of clustering altogether. If the maximum G_i^* occurs when the window size is small (i.e. 3x3) then maximum spatial autocorrelation occurs in close proximity to the centre pixel. If the maximum G_i^* occurs within a large analysis window (i.e. 9x9) then spatial dependence is more disparate.

RESULTS

Previous analysis (Derksen et al., 1998) used principal components analysis (PCA) to isolate temporally persistent snow cover patterns during the DJF 1988/89 time series. Four components were found to explain the majority of variance in the original data with the greatest amount of snow cover variability occuring in December. The four pentads which loaded most strongly to each component are summarized in Table 1. The focus of this study are the Getis images generated for these four pentads, which are shown in Figure 2.

The snow cover clusters in the Getis images were assigned to a class depending on the G_i^* values within the cluster. Level I clusters contain G_i^* values greater than or equal to 2, level II clusters are composed of G_i^* values between 1.5 and 2, while level III clusters contain G_i^* values between 1 and 1.5. This distinction allows both an examination of the evolution of snow cover clusters through the winter season, and an investigation of differences in orientation between high and low magnitude clusters.

Clusters in each level were isolated through a binary mask of the G_i^* values in the desired range. Cluster orientation was defined by applying a best fit line through the long axis of the cluster in question. A tally of orientations is shown in Table 2. Level I clusters have fewer modes of orientation then level II or III, with a high degree of inter-pentad variability existing between modes of orientation. For example, Feb. 10 - 14 is dominated by SW - NE oriented clusters (10 out of 13), while the December 27 to 31 clusters are scattered in their orientation (northeast to southwest; west to east; northwest to southeast) with no clear predominant direction of orientation. To understand this inter-pentad variability in cluster orientation requires the integration of atmospheric data.

500 mb geopotential height (500Z) and 700 mb temperature (700T) grids were contoured and overlaid on composite images of the three levels of Getis statistic clusters. No time lags were examined at the initial level of this study, the time period of the atmospheric fields corresponds exactly with the pentads of SWE data. The contour overlays are shown in Figures 3 through 6.

INTERPRETATION

The relationship between SWE Getis cluster orientation and atmospheric circulation is illustrated well in Figure 3. The February 10 to 14 SWE clusters show a meridional northwest to southeast orientation which corresponds exactly with the direction of atmospheric airflow as indicated by the 500Z contours. Some level III G_i^* clusters show a northeast to southwest orientation which corresponds to a zonal perturbation in the meridional temperature gradient visible in the 700T field.

The interpretation of results is complicated, however, by a comparison of Figures 3 (February 10 to 14) and 6 (December 7 to 11). Atmospheric conditions are similar during both pentads with strong meridional flow and a low pressure cell centred over the Eastern Arctic. A large proportion of level I G_i^* clusters can be observed in both pentads. The orientation of clusters between pentads is, however, dissimilar. Since the atmospheric variables at 500 and 700 mb respectively are inconclusive in providing a cause for the difference in cluster orientation, sea level pressure (SLP) grids were plotted for the December 7 to 11 and February 10 to 14 pentads to provide an additional means of explanation. The SLP fields are shown in Figure 7, and appear to be a modifying influence on cluster orientation. During February 10 to 14 (Figure 7b), the SLP, 500Z, and 700T fields show a similar meridional pattern over the

Table 1. Summary of PCA for Prairie SWE images

Component	*Variance Explained (%)*	*Pentad With Strongest Loading*	*Description*
PC 1	44	Feb. 10 - 14	Persistent snow cover, loads strongly through all of February
PC 2	20	Dec. 27 - 31	Late December accumulation pattern, loads strongly through January.
PC 3	17	Dec. 17 - 21	December accumulation pattern.
PC 4	11	Dec. 7 - 11	Early December accumulation pattern, little temporal persistence.

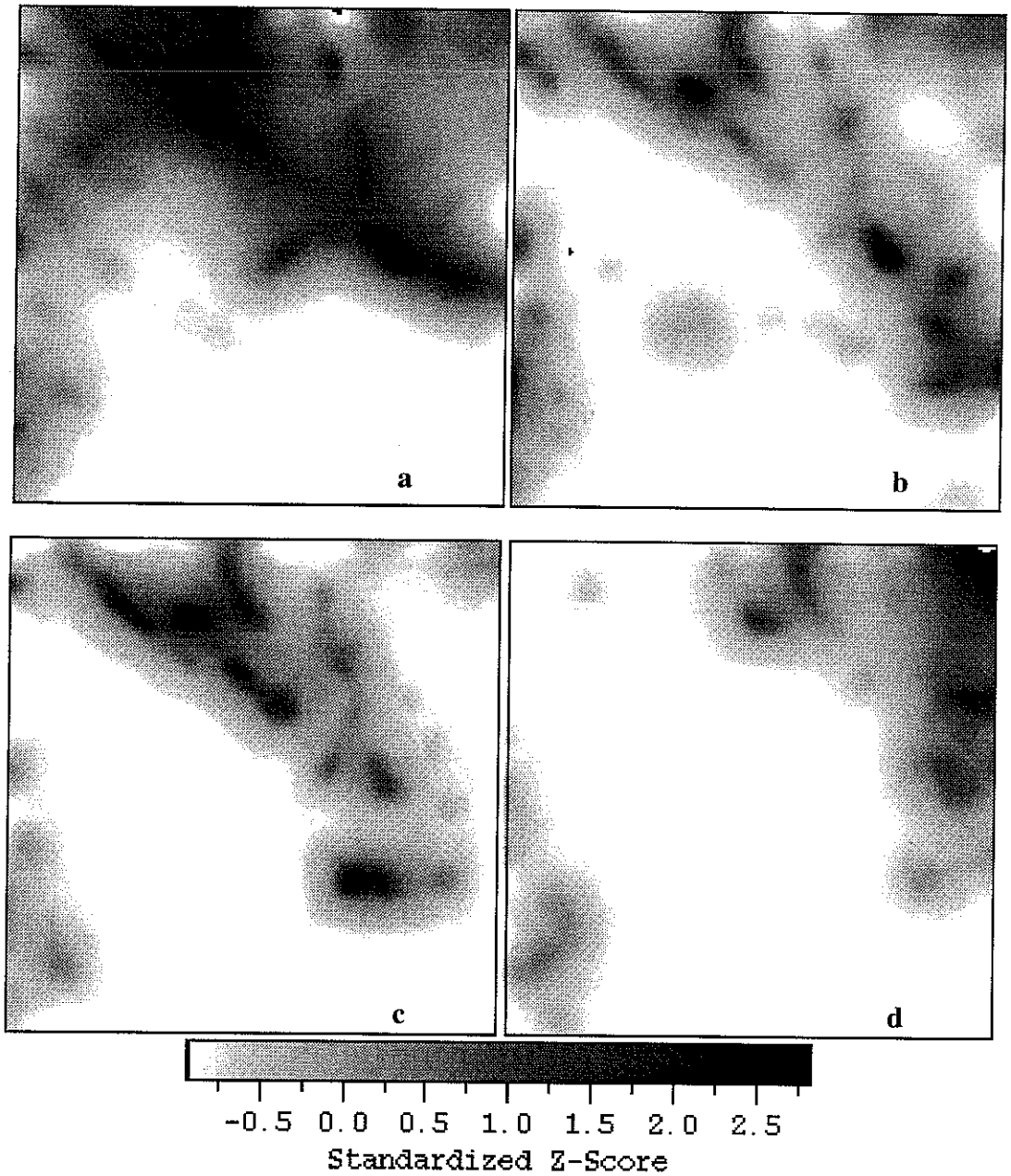

Figure 2. Getis images for (a) Feb. 10 - 14, (b) Dec. 27 - 31, (c) Dec. 17 - 21, and (d) Dec. 7 - 11. Darker tones indicate higher G_i clusters.*

Table 2. Cluster orientation within each pentad

	Level I		*Level II*		*Level III*	
Pentad	*Orientation*	*Count*	*Orientation*	*Count*	*Orientation*	*Count*
Feb. 10 - 14	NW - SE	3	NW - SE	2	NW - SE	5
			N - S	2	NE - SW	1
Dec. 27 -31	NW - SE	1	NW - SE	3	NW - SE	4
	W - E	1	NE - SW	2	NE - SW	2
			W - E	1		
Dec. 17 - 21	W - E	2	NW - SE	4	NW - SE	3
	NW - SE	1	W - E	2	W - E	1
Dec. 7 - 11	W - E	2	W - E	2	W - E	1
			N - S	1	N - S	2
			NW - SE	1		

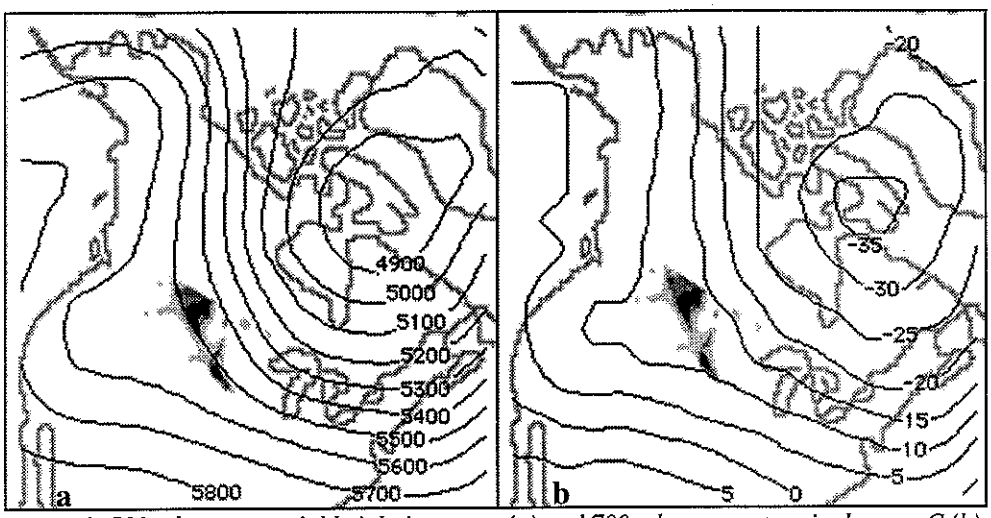

Figure 3. 500 mb geopotential height in metres (a) and 700 mb temperature in degrees C (b) overlaid on level I, II, and III clusters for the February 10 to 14 pentad. Level I clusters appear black, level II dark gray, and level III light gray.

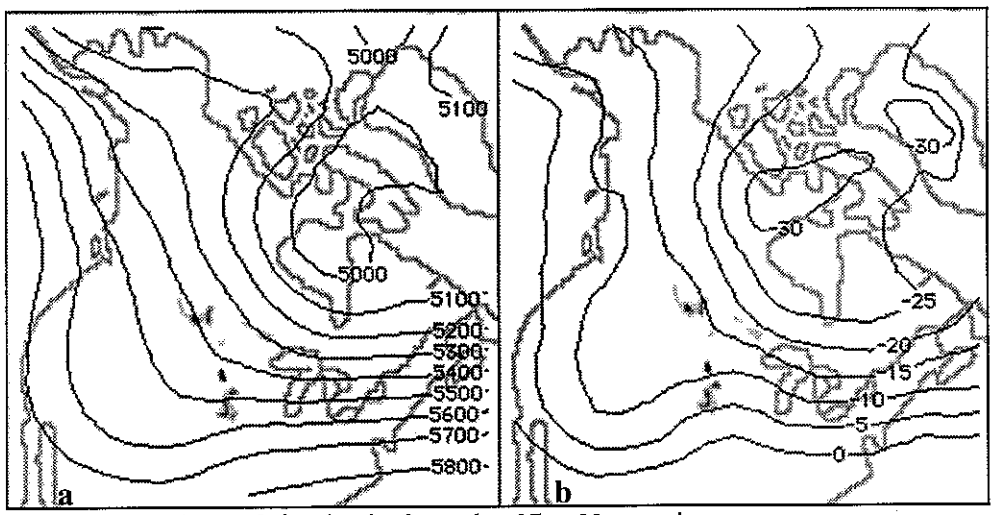

Figure 4. As in Figure 3, but for the December 27 to 31 pentad.

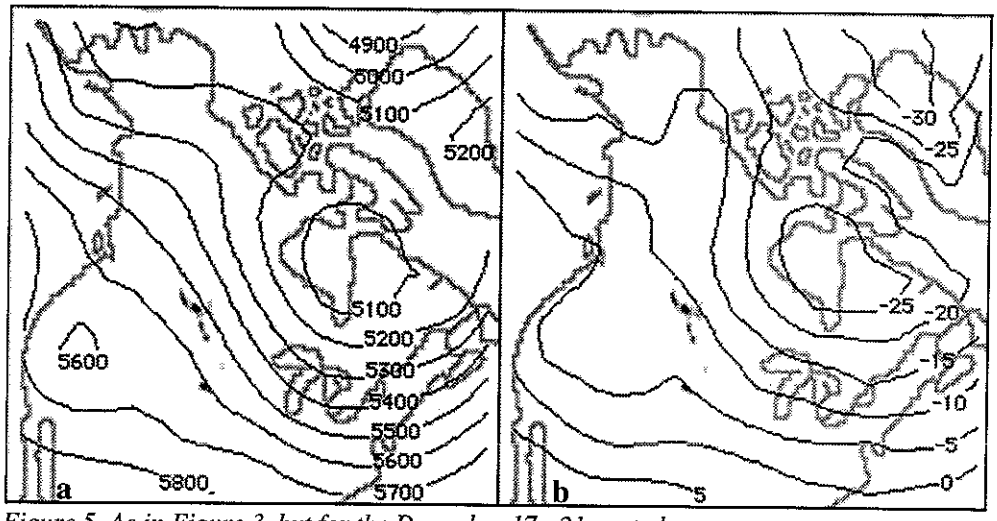

Figure 5. As in Figure 3, but for the December 17 - 21 pentad.

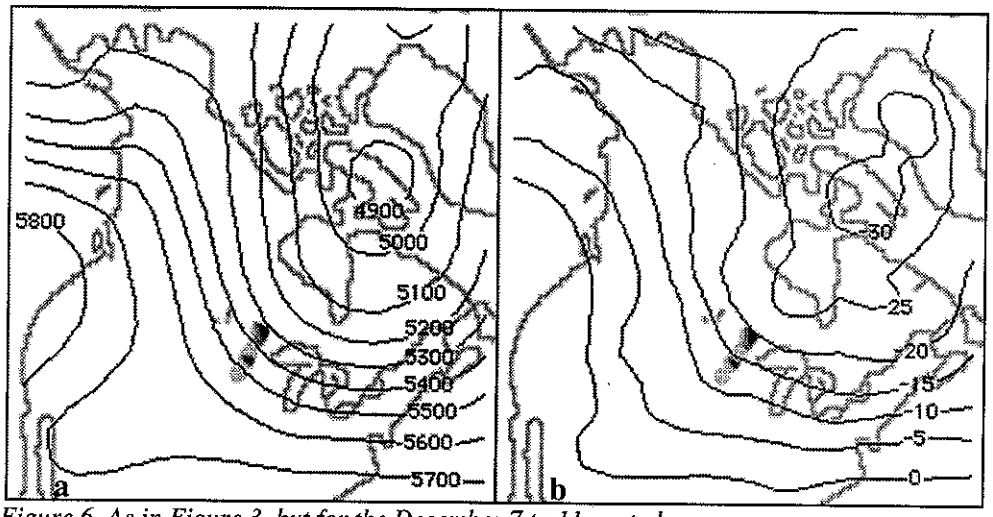

Figure 6. As in Figure 3, but for the December 7 to 11 pentad.

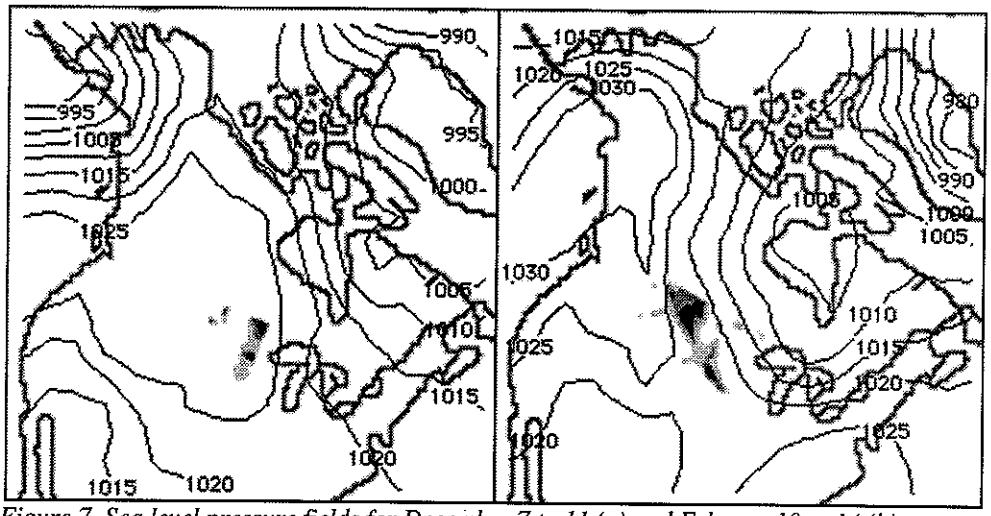

Figure 7. Sea level pressure fields for December 7 to 11 (a) and Febuary 10 to 14 (b).

Prairie study area. Correspondingly, the Getis clusters are oriented in the same meridional manner. Conversely, during December 7 to 11 (Figure 7a), the SLP field is more dissimilar to the 500Z pattern, while the 700T pattern is affected by a subtle outbreak of cold polar air from an Eastern Arctic low. The inconsistency in structure between the three atmospheric variables during December 7 to 11 may explain why the Getis cluster orientation does not match the direction of atmospheric airflow.

An additional explanation could involve the timing of the snow deposition events. If snow falls during a given pentad, G_i* clusters can be expected to be oriented with atmospheric flow as the depositional system moves across the Prairies. If precipitation does not occur within a pentad, localized climatic variables may play a greater role in modifying snow cover, thereby weakening the relationship between G_i* clusters and the synoptic state of the atmosphere. Time lagged analysis may also help clarify this issue, but is beyond the scope of this study.

700 mb temperature is observed to modify cluster magnitude between pentads. The December 27 to 31 and December 17 to 21 pentads (Figures 4 and 5) have very few pixels in level I clusters. These pentads also correspond temporally with warmer conditions over the study area. During December 27 to 31, and December 17 to 21, the -5 °C isotherm serves as the southern boundary to Getis clusters as opposed to the -10 °C isotherm during the other two pentads. This indicates that greater snow cover, as expressed through high G_i* clusters, corresponds to periods of lower atmospheric temperatures, a conclusion consistent with other empirical studies (for example Walsh et al., 1982; Namias, 1985).

DISCUSSION

This study represents the initial attempt to apply spatial dependence information in the form of the Getis statistic to passive microwave derived SWE imagery. It proves to be an effective analysis tool, both to visualize the spatially structured clusters inherent in the SWE data, and to quantify the magnitude of SWE values which compose each cluster. Subsequent research will apply the Getis statistic to multiple winters of data, facilitating an interannual comparison. Interpretation of future results will also focus not only on the maximum calculated G_i* values, but the distance from the centre pixel at which the maxima occur.

The results of this study indicate that the direction of atmospheric airflow as expressed by the 500 mb geopotential height field corresponds to the orientation of surface snow cover clusters with no time lag (Figures 3, 4, and 5). When the Getis clusters do not match the 500Z field (Figure 6), sea level pressure is identified as influencing cluster orientation (Figure 7). The 700 mb temperature field is also a controlling influence on the snow cover clusters both by modifying cluster orientation, and reinforcing cluster magnitude. Colder atmospheric temperatures are associated with increased snow accumulation as expressed through clusters of high G_i* values.

Clarifying these relationships will begin the process of exploiting the predictive potential in this method of analysis: the incorporation of time lags into the investigation of SWE G_i* clusters and atmospheric variables will lead to an understanding of the relative controlling influences of the atmosphere on snow accumulation patterns. The spatial component of the interpretation, through the use of the Getis statistic, can provide important information with respect to hydrological monitoring and climatological studies.

ACKNOWLEDGEMENTS

This work was supported by funding through the Canadian Atmospheric Environment Service Science Subvention and CRYSYS contract to E. LeDrew, and the Natural Science and Engineering Research Council (Operating Grant - E. LeDrew; Scholarship - C. Derksen). Thanks are extended to Joe Piwowar and Craig Smith for assistance with data preparation. The SSM/I EASE-Grid data were obtained from the EOSDIS National Snow and Ice Data Center Distributed Active Archive Center (NSIDC DAAC), University of Colorado at Boulder.

REFERENCES

Anselin, L. 1995. Local indicators of spatial association - LISA. Geographical Analysis. 27(2): 93-115.

Armstrong, R., A. Chang, A. Rango and E. Josberger. 1993. Snow depths and grain-size relationships with relevance for passive microwave studies. Annals of Glaciology. 17: 171-176.

Brown, R., and B. Goodison. 1996. Interannual variability in reconstructed Canadian snow cover, 1915-1992. Journal of Climate. 9: 1299-1318.

Cess, R., and 32 others. 1991. Interpretation of snow-climate feedback as produced by 17 general circulation models. Science. 253: 888-892.

Chang, A., J. Foster, and D. Hall. 1987. Nimbus-7 SMMR derived global snow cover parameters. Annals of Glaciology. 9: 39-44.

Cohen, J. 1994. Snow cover and climate. Weather. 49(5): 150-156.

Colbeck, S. 1987. A review of the metamorphism and classification of seasonal snow cover crystals. IAHS Publication 162: 3-34.

Derksen, C., E. LeDrew, and B. Goodison. 1998. SSM/I derived snow water equivalent data: the popential for investigating snow cover and atmospheric dynamics. Atmosphere-Ocean. In press.

Flato, G. 1997. The sensitivity of models in the SIMIP hierarchy to thermodynamic perturbations. In Villinger, T. (ed). Papers from the World Climate Research Program (WCRP) Conference on Polar Processes and Global Climate. Washington, November, 1997.

Getis, A., and J. Ord. 1992. The analysis of spatial association by distance statistics. Geographical Analysis. 24(3): 189-206.

Goodchild, M. 1986. Spatial Autocorrelation. Norwich: GeoBooks.

Goodison, B., I. Rubinstein, F. Thirkettle, and E. Langham. 1986. Determination of snow water equivalent on the Canadian prairies using microwave radiometry. Modelling Snowmelt Induced Processes, Proceedings of the Budapest Symposium, July 1986. 163-173.

Goodison, B. 1989. Determination of areal snow water equivalent on the Canadian Prairies using passive microwave satellite data. In Proceedings, IGARSS'89, Vancouver. 3:1243-1246.

Goodison, B., and A. Walker. 1994. Canadian development and use of snow cover information from passive microwave satellite data. In ESA/NASA International Workshop, Passive microwave remote sensing of land-atmosphere interactions. Saint Lary, France, January, 1993. 245-262.

Grody, N., and A. Basist. 1996. Global identification of snowcover using SSM/I measurements. IEEE Transactions on Geosciences and Remote Sensing. 34(1):237-249.

Hall, D., M. Sturm, C. Benson, A. Chang, J. Foster, H. Garbeil, and E. Chacho. 1991. Passive microwave remote and in situ measurements of Arctic and Subarctic snow covers in Alaska. Remote Sensing of Environment. 38: 161-172.

Karl, T., P. Groisman, R. Knight, and R. Heim. 1993. Recent variations of snow cover and snowfall in North America and their relation to precipitation and temperature variations. Journal of Climate. 6:1327-1344.

Kurvonen, L., and M. Hallikainen. 1997. Influence of land-cover category on brightness temperature of snow. IEEE Transactions on Geoscience and Remote Sensing. 35(2): 367-377.

Leathers, D., and D. Robinson. 1993. The association between extremems in North American snow cover extent and United States temperatures. Journal of Climate. 6(7): 1345-1354.

Namias, J. 1985. Some empirical evidence for the influence of snow cover on temperature and precipitation. Monthly Weather Review. 113: 1542-1553.

Ord, J., and A. Getis. 1995. Local spatial autocorrelation statistics: distributional issues and an application. Geographical Analysis. 27(6): 286-306.

Ulaby, F., and W. Stiles. 1980. The active and passive microwave response to snow parameters 2. Water equivalent of dry snow. Journal of Geophysical Research. 22(C2): 1045-1049.

Walker, A. 1993. Discrimination of a wet snow cover using passive microwave satellite data. Annals of Glaciology. 17: 307-311.

Walsh, J., D. Tucek, and M. Peterson. 1982. Seasonal snow cover and short-term climatic fluctuations over the United States. Monthly Weather Review. 110: 1474-1485.

Washington, W., and G. Meehl. 1986. General circulation model CO_2 sensitivity experiments: snow – sea ice albedo parameterizations and globally averaged surface air temperature. Climatic Change. 8: 231-241.

Wiesnet, D., C. Ropelewski, G. Kukla, and D. Robinson. 1987. A discussion of the accuracy of NOAA satellite-derived global seasonal snow cover measurements. In Goodison, B., R. Barry, and J. Dozier (eds.). Large Scale Effects of Seasonal Snow Cover, IAHS Publication 166: 291-304.

Wulder, M., and B. Boots. 1998. Local spatial autocorrelation characteristics of remotely sensed imagery assessed with the Getis statistic. International Journal of Remote Sensing. 19(11): 2223-2231.